Available online at www.sciencedirect.com

SciVerse ScienceDirect

Ceramics International 38 (2012) 5521–5526

CERAMICS INTERNATIONAL

www.elsevier.com/locate/ceramint

Characterizations and optical properties of Sm^{3+}-doped Sr_2SiO_4 phosphors

Myoung Gyu Ha [a], Jae-Sun Jeong [a], Kyoung-Rim Han [a], Yangsoo Kim [b], Ho-Soon Yang [c,**], Euh Duck Jeong [a], K.S. Hong [a,*]

[a] Division of High-Technology Materials Research, Korea Basic Science Institute, Pusan 618-230, Republic of Korea
[b] Sunchon Center, Korea Basic Science Institute, Sunchon 540-742, Republic of Korea
[c] Department of Physics, Pusan National University, Pusan 609-735, Republic of Korea

Received 8 March 2012; accepted 27 March 2012
Available online 2 April 2012

Abstract

Optical properties of samarium-doped strontium orthosilicate for near ultra-violet excitation are studied. Sr_2SiO_4:Sm^{3+} phosphor is synthesized by using the solid-state reaction method. The structure and physical properties of the phosphor are characterized by using X-ray diffractometer, scanning electron microscope, UV–visible spectrophotometer, high-resolution secondary ion mass spectrometer, and X-ray photoelectron spectrometer. Optical properties are studied by taking excitation and emission spectra. A strong red-orange luminescence corresponding to $^4G_{5/2} \rightarrow {}^6H_{7/2}$ transition of Sm^{3+} for near ultra-violet excitation is observed. It is found that Sr_2SiO_4:Sm^{3+} is a red-orange emitting phosphor and has higher efficiency for the operation with near ultra-violet excitation.

Keywords: Sr_2SiO_4; Sm^{3+}; Solid state reaction; Red-orange emission; Near ultraviolet excitation

1. Introduction

Rare-earth ions-doped materials have been studied extensively because they can be applied to plasma display panels, field emission displays, light-emitting diodes (LEDs), cathode ray tubes, and optoelectronic devices [1–3]. White LEDs have attracted lots of attention because of their potential applications such as backlights and lighting systems. White LEDs with phosphor materials are widely applied to lighting systems because of low energy consumption, small size, light weight, and long lifetime [4,5]. Above all, white LEDs are eco-friend and compact. Thus many studies for the rare-earth ions-doped materials are in progress to apply for white LEDs.

Recently rare-earth ions-doped alkaline-earth orthosilicates have attracted lots of attention because of promising luminescent properties and potential applications to white LEDs [6–9]. Strontium orthosilicate (Sr_2SiO_4) has attracted attention because of special structure features and excellent physical and chemical stability [10–15]. Sr_2SiO_4 absorbs ultra-violet (UV) radiation and emits white light when activated by Eu^{2+} ions [16], while shows intense emission when activated by Eu^{3+} ions [7,17]. Sr_2SiO_4 has two crystallographic phases, monoclinic-structured β-Sr_2SiO_4 and orthorhombic-structured α′-Sr_2SiO_4, of which the transition temperature is about 383 K [18]. There are two cation sites of Sr^{2+} in Sr_2SiO_4. Sr(I) is ten-coordinated and Sr(II) is nine-coordinated by oxygen ions [18,19]. These two different sites are equally distributed in the lattice [20].

Among the rare-earth ions, Sm^{3+} is an important activator for many different inorganic lattices producing red-orange emission due to its $^4G_{5/2} \rightarrow {}^6H_J$ ($J = 5/2$, 7/2, and 9/2) transitions, and adopted as an activator to determine the spectroscopic properties of long persistent phosphor [21–25]. In this article, we report a red-orange emission in Sm^{3+}-doped Sr_2SiO_4 prepared by using solid state reaction method. We characterized the crystallinity, morphology, elemental acquisition images, and chemical states of ions. We studied optical properties by taking absorption, excitation, and emission spectra with the concentrations of Sm^{3+}. We showed that Sr_2SiO_4:Sm^{3+} is a red-orange emitting phosphor and has higher efficiency for operation under near UV excitation, and can be a promising candidate for photonic applications.

* Corresponding author. Tel.: +82 51 974 6106; fax: +82 51 974 6116.
** Corresponding author. Tel.: +82 51 510 2221; fax: +82 51 513 7664.
E-mail addresses: hsyang@pusan.ac.kr (H.-S. Yang), kyongsoo@kbsi.re.kr (K.S. Hong).

0272-8842/$36.00
http://dx.doi.org/10.1016/j.ceramint.2012.03.067

2. Experimental details

$Sr_2SiO_4:Sm^{3+}$ phosphors were synthesized by using the solid state reaction method. The used starting materials were strontium carbonate ($SrCO_3$, Aldrich, 99.0%), silicon dioxide (SiO_2, Aldrich, 99.9%), and samarium oxide (Sm_2O_3, Aldrich, 99.9%). We kept the mole ratio of $SrCO_3$ and SiO_2 as 2:1 during the sample preparation process because we could observe [Sr_2SiO_4] phase. The concentrations of Sm^{3+} ions were varied from 0.1 mole% to 7.0 mole% while the amount of $SrCO_3$ and SiO_2 were fixed to 2 moles and 1 mole in all samples. The materials were ball-milled thoroughly in ethanol for 24 h for homogeneous mixing of small amount of activators. They were dried at 100 °C for 24 h and sintered at 1300 °C for 4 h in atmosphere. The materials were cooled down to room temperature quickly to avoid forming of other phases, and then crushed into a fine powder with an agate mortar and pestle. The synthesized powders were characterized by using the conventional X-ray diffractometer (XRD, Rigaku D-2400), scanning electron microscope (SEM, Coxem CX-100S), high-resolution secondary ion mass spectrometer (nano-SIMS, Cameca NS50), and X-ray photoelectron spectrometer (XPS, Escalab 250).

The nano-SIMS analysis was performed by using cesium primary ion beam with a diameter 100 nm, impact energy 16.0 keV, and a beam current 1.0 pA in order to obtain the optimized acquisition images. The raster size was 30 μm × 30 μm in all images and stepped over the sample in 256 pixels × 256 pixels to generate qualitative secondary ion images. The counting time was 10 ms/pixel. Samples were also simultaneously imaged using the secondary ions that were detected by an electron multiplier.

The synthesized powder was pressed into a pellet for the absorption and photoluminescence (PL) measurements. Absorption spectra were taken by using UV–visible spectrophotometer (Varian Cary300). PL spectra were taken with a steady-state fluorescence system with a 450 W Xe-lamp. The excitation light from the Xe-lamp (Muller Electronik-Optik LAX-1000) selected by using a 320 mm focal length monochromator (Dongwoo DM320i) was focused onto the sample. Fluorescence from the sample was collimated and refocused into the emission monochromator (Dongwoo DM320i) with a 320 mm focal length. PL was detected by using a photomultiplier tube (PMT, Hamamatsu R955) after passing the cut-off filter (Edmund OG 515) and was accumulated with a computer. All spectra were taken at room temperature.

3. Results and discussion

We have tried several temperatures with different sintering times to obtain the best crystallization conditions for each Sm^{3+} concentration. By checking the synthesized samples via XRD and PL measurements, we found that the best sintering conditions for our $Sr_2SiO_4:Sm^{3+}$ phosphors were 1300 °C and 4 h. The α′-Sr_2SiO_4 phase was observed at all samples prepared with different sintering temperatures and sintering times, and the samples synthesized with this condition showed the strongest PL intensity. Therefore we will discuss the samples prepared with this sintering condition throughout this article.

Fig. 1 shows XRD patterns of $Sr_2SiO_4:Sm^{3+}$ phosphors of (a) 0.1 mole%, (b) 1.5 mole%, and (c) 7.0 mole%. Figs. 1(d) and (e) are orthorhombic-structured α′-Sr_2SiO_4 and monoclinic-structured β-Sr_2SiO_4 patterns, respectively, from the JCPDS [26] shown for comparison. The observed diffraction patterns of $Sr_2SiO_4:Sm^{3+}$ phosphors are quite similar to the orthorhombic structure with a space group Pnma. However, some of monoclinic β-Sr_2SiO_4 phase patterns were observed (indicated by vertical arrows) in all concentrations of Sm^{3+}. Although the β-Sr_2SiO_4 peaks are observed, the major phase of the synthesized phosphors is determined as α′-Sr_2SiO_4. Since the ionic radii of metal ions are 1.16 Å on 6CN for Sr^{2+}, 0.96 Å on 6CN for Sm^{3+}, and 0.26 Å on 4CN for Si^{4+}. From the obtained patterns, we think that some Sm^{3+} ions are substituted into Sr^{2+} sites and some are in interstitial states of other ions. Further works are in progress to improve the purity of the obtained phosphors.

Fig. 2 shows SEM images of $Sr_2SiO_4:Sm^{3+}$ phosphors of concentrations (a) 0.1 mole% and (b) 5.0 mole%. We checked all phosphors and found almost uniform structure with grain size of about one micrometer regardless of Sm^{3+} concentrations.

The nano-SIMS is a powerful tool in elemental analysis by tracing a small amount of elements and isotopes at high spatial resolutions. The nano-SIMS offers the possibility of imaging components based on the elemental or isotopic compositions of their atomic and molecular ion fragments with high lateral resolution and sensitivity, yielding information that can complement other analytical methods, including many other types of SIMS experiments [27,28]. Above all, the nano-SIMS provides the capability of recording five atomic mass images together simultaneously with a high spatial resolution of 50 nm. These characteristics have made nano-SIMS a standard tool for the materials study, and nano-SIMS can compare elemental distributions exactly at a fixed position of the sample. Thus we used nano-SIMS to study the element compositional analysis.

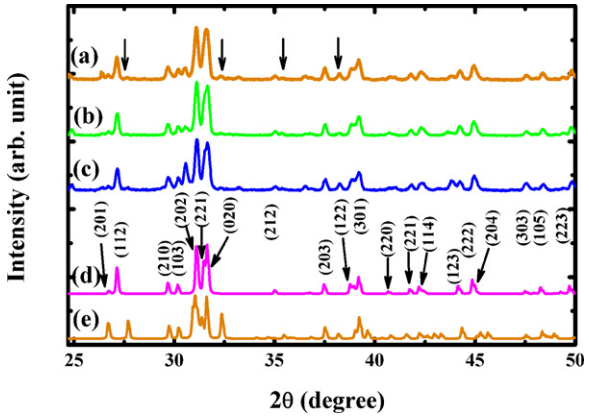

Fig. 1. XRD patterns of $Sr_2SiO_4:Sm^{3+}$ phosphors. Sm^{3+} concentrations are (a) 0.1 mole%, (b) 1.5 mole%, (c) 7.0 mole%, (d) orthorhombic-structured α′-Sr_2SiO_4, and (e) monoclinic-structured β-Sr_2SiO_4 from JCPDS. Upper patterns are shifted vertically for clarity.

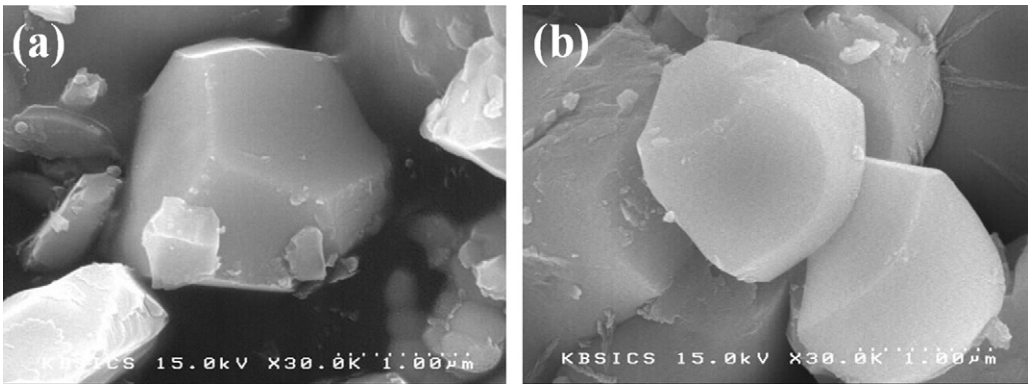

Fig. 2. SEM images of $Sr_2SiO_4:Sm^{3+}$ phosphors of concentrations (a) 0.1 mole% and (b) 5.0 mole%.

Fig. 3 shows the elemental acquisition images of (a) strontium, (b) silicon, (c) oxygen, and (d) samarium for the concentrations of 0.1 mole% (top) and 5.0 mole% (bottom), respectively. These elemental acquisition images were taken in high vacuum without etching the surface of the samples. The acquired elemental images showed that the elements were distributed throughout the samples. Since we could not obtain the reference samples, the obtained images provide only qualitative information of the elements. We could observe the existence of samarium even in lower concentrations. Thus we found that the high lateral resolution of the nano-SIMS could provide a unique tool for the investigation of elements in phosphor materials.

In order to see the chemical states of used elements including samarium, we took XPS spectra of the synthesized phosphors. Fig. 4 shows wide scan XPS spectra of $Sr_2SiO_4:Sm^{3+}$ phosphors. Sm^{3+} concentrations are (a) 0.1 mole%, (b) 1.0 mole%, (c) 2.5 mole%, and (d) 5.0 mole%. The elements such as C, Sr, Si, O, and Sm were observed in measurement. When the starting materials were burned in atmosphere like our sintering process, most of the oxygen and carbon from the starting materials were consumed during sintering process inside the furnace. Since XPS spectra were taken in vacuum without etching the surface of the samples, the observed carbon peaks were considered due to the atmospheric carbon during the measurement preparations.

We took narrow scan XPS spectra to each element for better understanding. Fig. 5 shows narrow scan XPS spectra of (a) strontium 3*d* states, (b) carbon 1*s* states, (c) samarium 3*d* states, and (d) silicon 2*p* states in $Sr_2SiO_4:Sm^{3+}$ phosphors. Sm^{3+} concentrations are 0.1 mole%, 1.0 mole%, 2.5 mole%, and 5.0 mole%, respectively, from top to bottom, in each figure. In Fig. 5(a), the peak positions for strontium 3*d* states (indicated by dotted line) were the same in all samples of different Sm^{3+} concentrations. This means that the binding energy does not change regardless of the amount of doped Sm^{3+} concentrations.

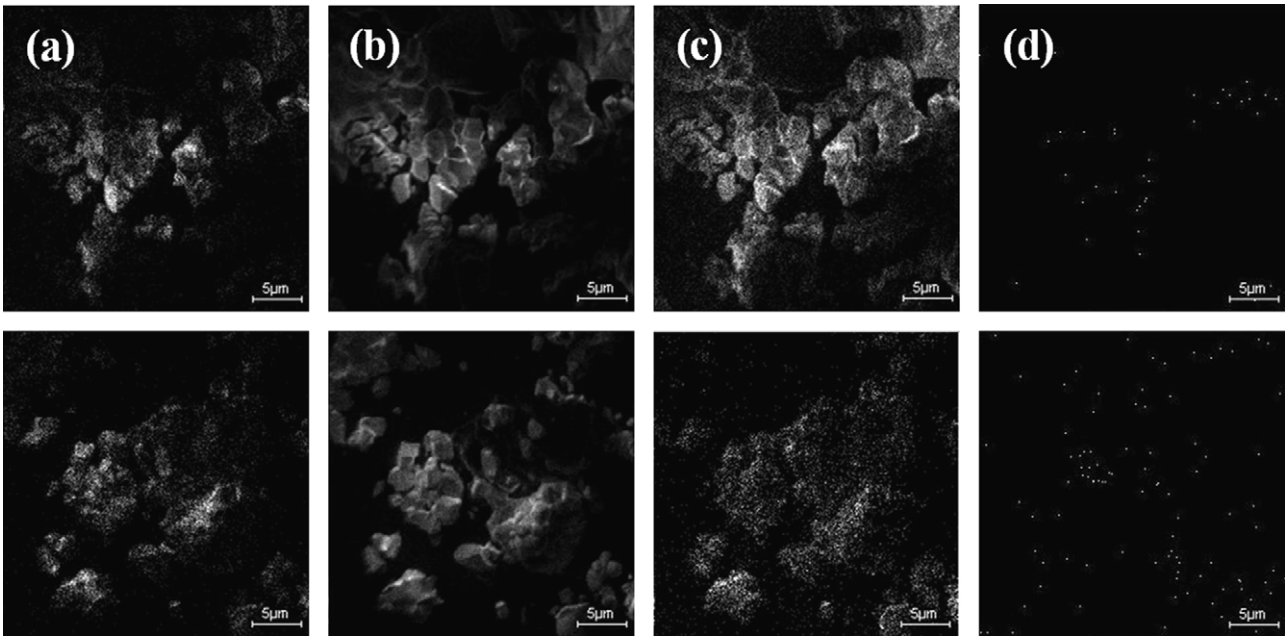

Fig. 3. Qualitative analysis for the elemental acquisition images of $Sr_2SiO_4:Sm^{3+}$ (a) strontium, (b) silicon, (c) oxygen, and (d) samarium ions for Sm^{3+} concentrations of 0.1 mole% (top) and 5.0 mole% (bottom), respectively.

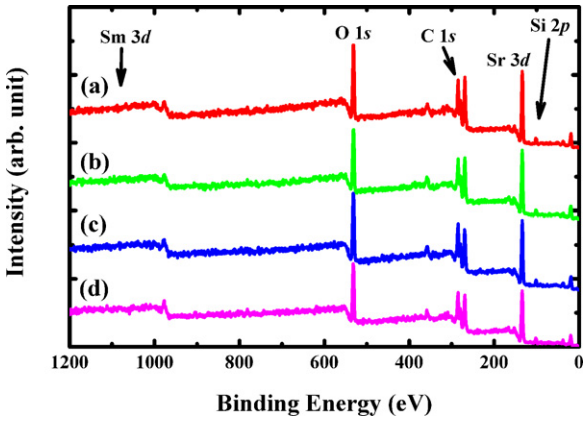

Fig. 4. Wide scan XPS spectra of Sr_2SiO_4:Sm^{3+} phosphors. Sm^{3+} concentrations are (a) 0.1 mole%, (b) 1.0 mole%, (c) 2.5 mole%, and (d) 5.0 mole%. Upper spectra are shifted vertically for clarity.

Fig. 5(b) shows the atmospheric carbon attached during the measurement preparation. Fig. 5(c) shows the variation of the doped amount of Sm^{3+} qualitatively in Sr_2SiO_4:Sm^{3+} phosphors according to the concentrations. Fig. 5(d) shows that the observed chemical state of silicon ions is Si^{4+} [29].

Fig. 6 shows UV–visible absorption spectrum of 7.0 mole% Sm^{3+}-doped Sr_2SiO_4 phosphor. For the samples of lower concentrations such as 1.0 mole%, the absorption was too weak to observe. A strong absorption band of NUV was observed around 402 nm corresponding to ${}^6H_{5/2} \rightarrow {}^4F_{7/2}$ from doped Sm^{3+} ions. Other observed absorption bands were identified to the electronic transitions such as ${}^6H_{5/2} \rightarrow {}^4D_{1/2}$ at 374 nm, ${}^6H_{5/2} \rightarrow ({}^6P,{}^4P)_{5/2}$ at 423 nm, and ${}^6H_{5/2} \rightarrow {}^4G_{9/2}$ at 440 nm [30]. Most of these bands were also observed in the excitation spectra which will be shown later. From these absorption bands, we understood that the luminescent properties were originated from the direct transitions from the ground state ${}^6H_{5/2}$ to the excited states of Sm^{3+}, not via the energy transfer processes [31].

Fig. 7 shows the excitation spectra of 7.0 mole% Sm^{3+}-doped Sr_2SiO_4 phosphor monitored at 598 nm emission. The identified excitation bands were ${}^4D_{3/2}$ at 360 nm, ${}^4D_{1/2}$ at 374 nm, ${}^4F_{7/2}$ at 402 nm, $({}^6P,{}^4P)_{5/2}$ at 413 nm, ${}^4G_{9/2}$ at 437 nm, ${}^4I_{13/2}$ at 460 nm, and ${}^4I_{11/2}$ at 478 nm [30]. All these bands were the transitions from the ground state, ${}^6H_{5/2}$, to the higher energy states of Sm^{3+}. Since the transition corresponding to ${}^6H_{5/2} \rightarrow {}^4F_{7/2}$ at 402 nm has the maximum intensity among these bands; the emission spectra are taken with the excitation from this band position. The transitions in these excitation spectra were closely correlated with those of absorption spectra in UV–visible region shown in Fig. 6.

Fig. 8 shows the emission spectra of Sr_2SiO_4:Sm^{3+} phosphors with the excitation of ${}^6H_{5/2} \rightarrow {}^4F_{7/2}$ at 402 nm. Sm^{3+} concentrations are (a) 2.5 mole% and (b) 1.5 mole%. The identified emission bands were by the intra 4*f* transitions of Sm^{3+} such as ${}^4G_{5/2} \rightarrow {}^6H_{5/2}$ at 561 nm, ${}^4G_{5/2} \rightarrow {}^6H_{7/2}$ at 598 nm, and ${}^4G_{5/2} \rightarrow {}^6H_{9/2}$ at 644 nm. Among these, the transition ${}^4G_{5/2} \rightarrow {}^6H_{7/2}$ has strongest intensity and this can be applied to the red-orange emitting display materials. The transition ${}^4G_{5/2} \rightarrow {}^6H_{7/2}$ satisfies the selection rule of $\Delta J = \pm 1$, where J is the angular momentum. Magnetic dipole transitions obey the selection rule of $\Delta J = 0$ and ± 1, and electric dipole transitions obey the selection rule of $\Delta J \leq 6$ unless J or $J' = 0$

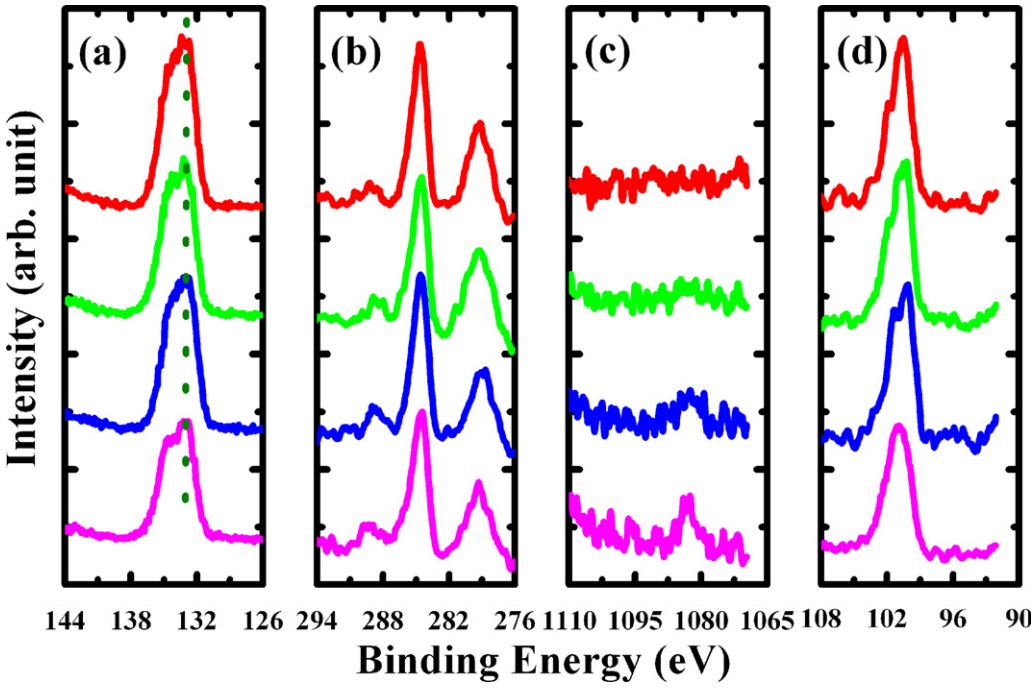

Fig. 5. Narrow scan XPS spectra of (a) strontium 3*d* states, (b) carbon 1*s* states, (c) samarium 3*d* states, and (d) silicon 3*p* states in Sr_2SiO_4:Sm^{3+} phosphors. Sm^{3+} concentrations are 0.1 mole%, 1.0 mole%, 2.5 mole%, and 5.0 mole%, respectively, from top to bottom in all three figures. Upper spectra are shifted vertically for clarity.

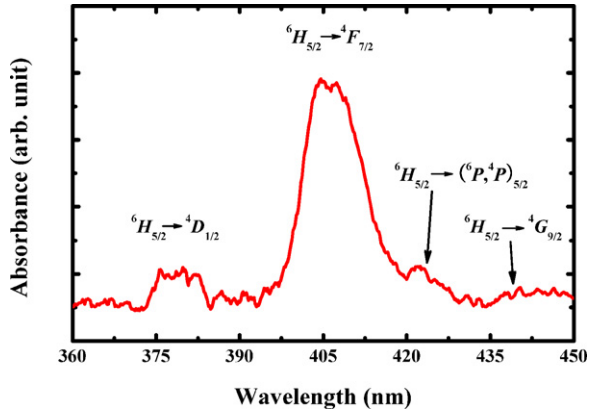

Fig. 6. UV–visible absorption spectra of 7.0 mole% Sm^{3+}-doped Sr_2SiO_4 phosphor.

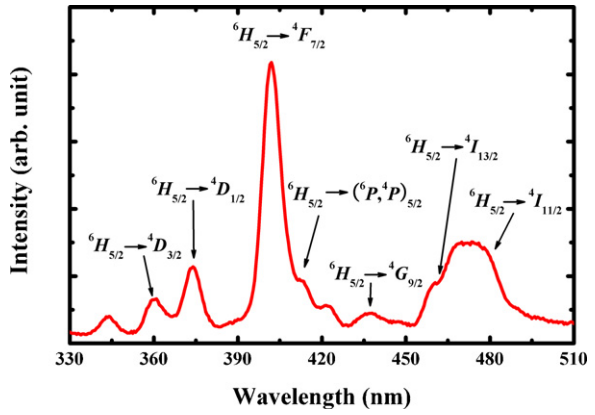

Fig. 7. Excitation spectra of 7.0 mole% Sm^{3+}-doped Sr_2iO_4 phosphor monitored at 598 nm emission.

when $\Delta J = 2,3,6$ [32]. The transitions $^4G_{5/2} \rightarrow {}^6H_{5/2}$ and $^4G_{5/2} \rightarrow {}^6H_{7/2}$ are magnetic dipole transitions, while the transition $^4G_{5/2} \rightarrow {}^6H_{9/2}$ is an electric dipole transition.

Consider the ratio between the intensities of the electric dipole transition and magnetic dipole transition. The local symmetry is measured with the relative intensities of these two transitions. The larger value of this ratio means more distortion from the inversion symmetry [33]. The obtained values were

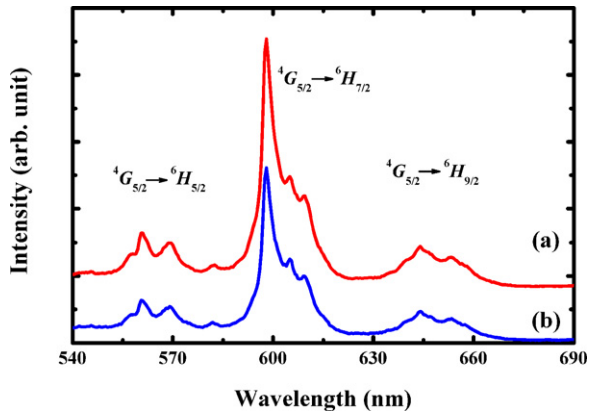

Fig. 8. Emission spectra of Sr_2TiO_4:Sm^{3+} phosphors with the excitation of $^6H_{5/2} \rightarrow {}^4F_{7/2}$ at 402 nm. Sm^{3+} concentrations are (a) 2.5 mole% and (b) 1.5 mole%. Upper spectra are shifted vertically for clarity.

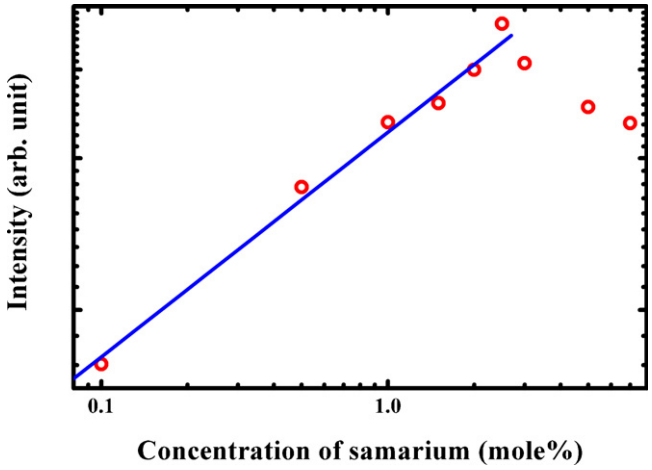

Fig. 9. Concentration dependence of emission intensities corresponding to $^4G_{5/2} \rightarrow {}^6H_{7/2}$ transition of Sm^{3+} in Sr_2SiO_4:Sm^{3+} phosphors based on Fig. 8. The straight line is a least square fit to the lower concentration data points.

kept almost constant between 5.65 and 6.48, which meant that the Sm^{3+} ions were quite distorted cation environments in Sr_2SiO_4 structures rather than in embedded states in Sr_2SiO_4 structure. The structural change can be monitored with the spectral width [34]. There was no significant change in the observed spectral widths for the samples in Fig. 8. Therefore there was no change in the structural environment around Sm^{3+} ions with increase of the concentration, which means that the synthesized Sr_2SiO_4:Sm^{3+} phosphors can be a promising candidate for photonic applications.

Although we showed the emission spectra of only two samples in Fig. 8, we could observe the same emission patterns in all synthesized samples. We plotted the intensities of the strongest emission peak of Sr_2SiO_4:Sm^{3+}, $^4G_{5/2} \rightarrow {}^6H_{7/2}$, according to the Sm^{3+} concentrations in log–log scale as shown in Fig. 9. The straight line is a least square fit to the data points of lower concentration. PL intensity increased almost linearly as the concentration increased up to 2.5 mole% and then decreased. We found that the best concentration of Sr_2SiO_4:Sm^{3+} phosphor for display applications is about 2.5 mole% in our phosphor system. The quenching of PL intensity with the Sm^{3+} concentration was attributed to a decrease in the number of optically active Sm^{3+} ions. Since we took all the spectra at room temperature, we could not confirm whether this decrease was due to thermal phonons or not.

4. Summary

We synthesized Sr_2SiO_4:Sm^{3+} phosphors by using the solid state reaction method and characterized their properties by using XRD, SEM, nano-SIMS, XPS, and UV–visible spectrophotometer. We studied their optical properties caused by the chemical compositions in red-orange emitting phosphors. The luminescent features were obtained by analyzing the variations in the emission and excitation spectra with the concentrations. We found that the red-orange emitting Sr_2SiO_4:Sm^{3+} phosphors could be a promising candidate for photonic applications.

Acknowledgment

This work was supported by Korea Basic Science Institute Grant C32223, and the Basic Science Research Program through NRF of Korea, 2009-0076635.

References

[1] L. Armelao, S. Quici, F. Barigelletti, G. Accorsi, G. Bottaro, M. Cavazzini, E. Tondello, Design of luminescent lanthanide complexes: from molecules to highly efficient photo-emitting materials, Coordination Chemistry Reviews 254 (2010) 487–505.

[2] J.C.G. Bünzli, S.V. Eliseeva, Lanthanide NIR luminescence for telecommunications, bioanalyses and solar energy conversion, Journal of Rare Earths 28 (2010) 824–842.

[3] S. Ye, F. Xiao, Y.X. Pan, Y.Y. Ma, Q.Y. Zhang, Phosphors in phosphor-converted white light-emitting diodes: recent advances in materials, techniques and properties, Materials Science and Engineering R 71 (2010) 1–34.

[4] H.V. Demir, S. Nizamoglu, T. Erdem, E. Mutlugun, N. Gaponik, A. Eychmuller, Quantum dot integrated LEDs using photonic and excitonic color conversion, Nano Today 6 (2011) 632–647.

[5] U. Lafont, H. van Zeijl, S. van der Zwaag, Increasing the reliability of solid state lighting systems via self-healing approaches: A review, Microelectronics Reliability 52 (2012) 71–89.

[6] W.H. Hsu, M.H. Sheng, M.S. Tsai, Preparation of Eu-activated strontium orthosilicate ($Sr_{1.95}SiO_4$:$Eu_{0.05}$) phosphor by a sol–gel method and its luminescent properties, Journal of Alloys and Compounds 467 (2009) 491–495.

[7] Y. Qiao, X. Zhang, X. Ye, Y. Chen, H. Guo, Photoluminescent properties of Sr_2SiO_4:Eu^{3+} and Sr_2SiO_4:Eu^{2+} phosphors prepared by solid-state reaction method, Journal of Rare Earths 27 (2009) 323–326.

[8] S.H. Lee, H.Y. Koo, Y.C. Kang, Characteristics of α′- and β-Sr_2SiO_4:Eu^{2+} phosphor powders prepared by spray pyrolysis, Ceramics International 36 (2010) 1233–1238.

[9] S. Kamei, Y. Kojima, N. Nishimiya, Preparation and fluorescence properties of novel red-emitting Eu^{3+}-activated amorphous alkaline earth silicate phosphors, Journal of Luminescence 130 (2010) 2247–2250.

[10] H. He, R. Fu, Y. Cao, X. Song, Z. Pan, X. Zhao, Q. Xiao, R. Li, $Ce^{3+} \rightarrow Eu^{2+}$ energy transfer mechanism in the Li_2SrSiO_4:Eu^{2+}, Ce^{3+} phosphor, Optical Materials 32 (2010) 632–636.

[11] H. Yu, Y. Lai, G. Gao, L. Kong, G. Li, S. Gan, G. Hong, Photoluminescence and energy transfer studies on Eu^{2+} and Ce^{3+} co-doped $SrCaSiO_4$ for white light-emitting-diodes, Journal of Alloys and Compounds 509 (2011) 6635–6639.

[12] V.P. Dotsenko, S.M. Levshov, I.V. Berezovskaya, G.B. Stryganyuk, A.S. Voloshinovskii, N.P. Efryushina, Luminescent properties of Eu^{2+} and Ce^{3+} ions in strontium litho-silicate Li_2SrSiO_4, Journal of Luminescence 131 (2011) 310–315.

[13] H. Yu, G. Gao, L. Kong, G. Li, S. Gan, G. Hong, Synthesis and luminescence properties of a novel red-emitting phosphor $SrCaSiO_4$:Eu^{3+} for ultraviolet white light-emitting diodes, Journal of Rare Earths 29 (2011) 431–435.

[14] T. Joseph, M.T. Sebastian, Microwave dielectric properties of alkaline earth orthosilicates M_2SiO_4 (M = Ba, Sr, Ca), Materials Letters 65 (2011) 891–893.

[15] L. Zhang, Z. Lu, H. Yang, P. Han, N. Xu, Q. Zhang, Preparation of Dy^{3+}-activated strontium orthosilicate (Sr_2SiO_4:Dy^{3+}) phosphors and its photoluminescent properties, Journal of Alloys and Compounds 512 (2012) 5–11.

[16] H. He, R. Fu, X. Song, D. Wang, J. Chen, White light-emitting $Mg_{0.1}Sr_{1.9}SiO_4$:Eu^{2+} phosphors, Journal of Luminescence 128 (2008) 489–493.

[17] J. Yang, L. Yang, W. Liu, Y. Zhang, H. Fan, Y. Wang, H. Liu, J. Lang, D. Wang, Luminescence behavior of Eu^{3+} in $CaSiO_3$:Eu^{3+} (Bi^{3+}) and Sr_2SiO_4:Eu^{3+} (Bi^{3+}), Journal of Alloys and Compounds 454 (2008) 506–509.

[18] M. Catti, G. Gazzoni, G. Ivaldi, G. Zanini, The β ↔ α′ phase transition of Sr_2SiO_4. I. Order-disorder in the structure of the α′ form at 383 K, Acta Crystallographica. Section B, Structural Science 39 (1983) 674–679.

[19] M. Catti, G. Gazzoni, G. Ivaldi, Structures of twinned β-Sr_2SiO_4 and of α′-$Sr_{1.9}Ba_{0.1}SiO_4$, Acta Crystallographica. Section C. Crystal Structure Communications 39 (1983) 29–34.

[20] N. Lakshminarasimhan, U.V. Varadaraju, Luminescence and afterglow in Sr_2SiO_4:Eu^{2+}, RE^{3+} [RE = Ce, Nd, Sm and Dy] phosphors – role of co-dopants in search for afterglow, Materials Research Bulletin 43 (2008) 2946–2953.

[21] Z. Xu, X. Kang, C. Li, Z. Hou, C. Zhang, D. Yang, G. Li, J. Lin, Ln^{3+} (Ln = Eu, Dy, Sm, and Er) ion-doped YVO_4 nano/microcrystals with multiform morphologies: hydrothermal synthesis, growing mechanism, and luminescent properties, Inorganic Chemistry 49 (2010) 6706–6715.

[22] B. Lei, S.Q. Man, Y. Liu, S. Yue, Luminescence properties of Sm^{3+}-doped $Sr_3Sn_2O_7$ phosphor, Materials Chemistry and Physics 124 (2010) 912–915.

[23] Z.H. Ju, S.H. Zhang, X.P. Gao, X.L. Tang, W.S. Liu, Reddish orange long afterglow phosphor Ca_2SnO_4:Sm^{3+} prepared by sol–gel method, Journal of Alloys and Compounds 509 (2011) 8082–8087.

[24] G. Tang, H. Xiong, W. Chen, L. Luo, The study of Sm^{3+}-doped low-phonon-energy chalcohalide glasses, Journal of Non-Crystalline Solids 357 (2011) 2463–2467.

[25] X. Lin, X. Qiao, X. Fan, Synthesis and luminescence properties of a novel red $SrMoO_4$:Sm^{3+}, R^+ phosphor, Solid State Sciences 13 (2011) 579–583.

[26] Inorganic Crystal Structure Database, http://http://icsd.fiz-karlsruhe.de.

[27] M.L. Kraft, S.F. Fishel, C.G. Marxer, P.K. Weber, I.D. Hutcheon, S.G. Boxer, Quantitative analysis of supported membrane composition using the nano-SIMS, Applied Surface Science 252 (2006) 6950–6956.

[28] S.G. Boxer, M.L. Kraft, P.K. Weber, Advances in imaging secondary ion mass spectrometry for biological samples, Annual Review of Biophysics 38 (2009) 53–74.

[29] J.F. Moulder, W.F. Stickle, P.E. Sobol, K.D. Bomben, in: J. Chastain, R.C. King, Jr. (Eds.), Handbook of X-ray Photoelectron Spectroscopy, Physical Electronics Inc., Minnesota, 1995.

[30] W.T. Carnall, H. Crosswhite, H.M. Crosswhite, Argonne Report ANL-78-95 (1978).

[31] H. Zhang, X. Fu, S. Niu, Q. Xin, Synthesis and photoluminescence properties of Eu^{3+}-doped $AZrO_3$ (A = Ca, Sr Ba) perovskite, Journal of Alloys and Compounds 459 (2008) 103–106.

[32] Z. Cui, R. Ye, D. Deng, Y. Hua, S. Zhao, G. Jia, C. Li, S. Xu, Eu^{2+}/Sm^{3+} ions co-doped white light luminescence $SrSiO_3$ glass-ceramics phosphor for white LED, Journal of Alloys and Compounds 509 (2011) 3553–3558.

[33] R.K. Brow, D.R. Tallant, G.L. Turner, Raman and 11B nuclear magnetic resonance spectroscopic studies of alkaline-earth lanthanoborate glasses, Journal of the American Ceramic Society 79 (1996) 2410–2416.

[34] B. Henderson, G.F. Imbusch, Optical Spectroscopy of Inorganic Solids, Clarendon Press, Oxford, 1989.